

Numerical Thermohydraulic Analysis of Flow Boiling in Geometrical-Modified Microchannels

O. T. Olakoyejo^{1*}, S. A. Okon¹, O. O. Adewumi¹, Sogo Abolarin², A.O Adelaja¹, A. I. Fetuga¹, A.S. Shote³, S.A. Aasa^{3,4}

¹Department of Mechanical Engineering, University of Lagos, Nigeria

²Department Engineering Sciences, University of the Free State, Bloemfontein, South Africa

³Department of Mechanical Engineering Olabisi Onabanjo University,

⁴Department of Mechanical and Aeronautical Engineering, University of Pretoria, South Africa

*Email: oolakoyejo@unilag.edu.ng

Abstract

One of the major issues of flow boiling in microchannels is ensuring adequate management of thermohydraulic instabilities which severely impact the system's efficiency in terms of pressure drop and heat transfer coefficient (HTC). The current study focuses on microchannels with geometric modifications, varying inlet conditions and geometry dimensions with view on mitigating thermohydraulic instabilities and improving overall performance. The study used Computational fluid dynamics (CFD) software - ANSYS Fluent - with the Volume of Fluid (VOF) model to simulate the flow boiling in microchannels. The flow is transient and laminar in a 3-D domain with water (H₂O-liquid) as working fluid. The flow and heat transfer characteristics in baseline rectangular are compared with constricted inlet-, and expanding inlet microchannels. Pressure drop, heat transfer coefficient, Nusselt number, and frictional factor are studied and visualized across varying mass fluxes 3000 – 7000 kg/m²s (for all microchannels) and angle of divergence 0.2° – 1° (for the expanding inlet). The expanding inlet microchannel showed a better thermohydraulic performance, having a 63.25% increase in HTC and a 64.16% reduction in pressure drop compared to the baseline design, highlighting its potential for enhancing thermohydraulic stability. Also, the angle of divergence gave more insights to the expanding inlet microchannel with 0.2° having a better performance. These findings solidify the critical role of geometric modifications in optimizing microchannel performance, with the expanding inlet design resulting as the configuration for a better heat transfer performance and pressure stability, thus giving valuable insights for advancements in microchannel design and flow boiling applications.

Keywords: Boiling, microchannel, ANSYS, CFD, thermohydraulic, working fluid

1.0 INTRODUCTION

The concept of boiling in heat transfer is regarded as an important occurrence in processes involving transfer of heat. Most especially in systems like heat exchangers in boiler tubes, evaporators, and some other chemical processes of industrial applications (Sun *et al.*, 2014). Boiling in these thermal systems entails a phase change of working fluid from liquid to vapor. As would be seen in this study, more focus will be centered on flow boiling.

Flow boiling is a process of heat transfer that occurs from a liquid to a vapor phase change of a fluid passing through a channel. Several articles have established this phenomenon and carried out simulations herein (Li *et al.*, 2022, 2023).

Studies have shown flow boiling to exist in applications with high heat flux (Mudawar, 2011). Despite the consequential research over the past decade, there are still challenges relating to achieving the peak of thermohydraulic performance of these systems. The thermohydraulic instabilities such as reduced flow rates, low thermal performance, pressure drop fluctuations, remain a major research barrier. Factors contributing to these instabilities include rapid bubble growth, flow pattern transitions, and thermal dynamics within the microchannels (Karayiannis and Mahmoud, 2017).

Literature have highlighted the prevalence of thermohydraulic instabilities in microchannel flow boiling. Kamel *et al.* (2019) laid emphasis on the need for enhanced heat transfer techniques in high heat flux systems. Mudawar (2011, 2013) pointed out the limitations of single-phase

systems in the scope of the cooling requirements for developing technologies, hence the further need for research into multi-phase flow boiling. Understanding these instabilities is not just theoretical but has several practical implications for the advancement of physics behind two-phase flow, efficiency improvement in cooling systems and more reliable heat transfer management in critical sectors using high technologies (Cukrov *et al.*, 2017).

Over the past few decades, researchers in the area of flow boiling have tried to understand the process associated with this phenomenon by analysing and making significant designs for optimum thermodynamics systems involving flow boiling which allows a good amount of heat transfer with flow boiling in microchannels established to have significant applications in the engineering world (Kamel *et al.*, 2019, Wang *et al.*, 2021, 2023).

Karayiannis and Mahmoud (2018) stated that flow boiling located at the heat source in mini to micro passages was confirmed as one way to remove increasing high heat fluxes generated as a result of these channels due to their elevated rate of heat transfer with little to no variation in surface temperature. This relates to instabilities such as pressure drop in the channel geometries, and how these instabilities consequently affect the efficiency of this process.

Flow boiling can be sectioned into two concepts which are single phase and multi-phase flow systems with many researchers making efforts to identify the characteristics of these concepts in micro-scale systems (Hasselgreaves *et al.*, 2016, Özdemir and Sozbir, 2018, Kumar *et al.*, 2021). It would be fair to say that these systems each have their pros and cons. In single-phase systems, it is the inability to meet the cooling requirements of many applications due to the absurd rise in rate of heat loss. This is tied with the need to reduce the cooling aid's size employed. Few good examples of these applications are automobiles' heat exchangers, magnetohydrodynamic generator electrode walls, and nozzles in rocket engines (Mudawar, 2011). The ineffectiveness of single-phase systems has led to multi-phase system taking advantage of the high HTC associated with boiling and condensation. Major benefits accompanied by the multi-phase concept of flow boiling are related to mitigating the thermohydraulic instabilities such as increased Heat Transfer Coefficient, improved heat flux and, complex flow regimes (Mudawar, 2013).

Working fluids such as R134a and Cu-O nanofluid have found their applications in thermal systems involving flow boiling. Adio *et al.* (2021) investigated using nanofluid (Copper Oxide) as a cooling agent in the place of refrigerants (R134a, for example) and water (H₂O) in a manifold microchannel with the aim that nanofluids provides a better result. This study used a range of Reynolds number (100 – 400) and volume fraction of Cu-O nanoparticle from 0 – 4 %. The flow was considered laminar, steady, and incompressible and showed that the Nusselt number increased as Reynolds number increased. Across all volume fractions, the Nusselt number was maximum at Re = 400.

Ma *et al.* (2022) evaluated the characteristics of flow boiling of surfaces with extremely small pin-fins with mass flux values (200 – 500 kg/m²s) with inlet temperatures 30 – 50 °C and the working fluid as deionized water. Various characteristics like the boiling curves, HTC were plotted with ranges of heat flux, inlet temperature and mass flux. Some analysis drawn from this literature include the temperature of the wall increasing slightly as the heat flux increases.

Jia *et al.* (2018) performed experiments on a porous wall microchannel. The working fluid employed was pure acetone liquid. The inlet temperature set as 30 °C and ranging mass flux 255 – 843 kg/m²s. The analysis drawn from this experiment showed that porous wall microchannels improve heat flux in comparison to rectangular channels. Balasubramanian *et al.* (2022) reviewed flow characteristics and mechanisms of these characteristics. It was evaluated that the design parameters and HTC of the microchannel are crucial to applicable flow structures.

Zhang *et al.* (2017) compared results between micro-grooved channels having re-entrant cavity array and without re-entrant cavity array (MGRA and MG, respectively) employing deionized water. Results such as HTC performance and the PD were analysed for both channels for the range of inlet temperature (10, 25, 40 °C). The study shows that HTC increased with mass flux. This literature showed that MGRA yielded a better pressure drop when compared to MG because of the cavity array. In summary, the concept of thermohydraulic properties involves the total understanding of various important parameters like HTC, CHF, vapor quality, and flow instabilities (Soliman *et al.*, 2018, Wlazlak *et al.*, 2018, Kamel *et al.*, 2019).

For these thermohydraulic instabilities, several papers have dug into how they can be mitigated. These instabilities could stem from rapid bubble growth which leads to reduction in flow rate, pressure increase or even reversal in flow (Mohammed *et al.*, 2019). Karayiannis and Mahmoud (2017) also stated additional reasons explaining some instabilities in microchannels. Several mitigating steps were taken such as placing inlet restrictors at the entrances of several parallel microchannels. This was done also to reduce instability (Liu *et al.*, 2022, 2023).

Lee *et al.* (2007) conducted experiments using straight & expanding microchannels. The expanding microchannels postulated an improved heat transfer performance. Mukherjee and Kandlikar (2009) also carried out simulations to study inlet restrictors' effects on the growth of singular vapor bubbles near the restricted end. Inference was drawn that these bubble growth rate decreased significantly with the smallest open area (4 %), i.e. smaller ratios proved more effective in reducing flow reversal in the channel. This was as a result of increasing liquid velocities and significant pressure drops. It is important to note that several papers that focused on multiphase microchannel flows also employed the VOF model in their simulations (Yogesh *et al.*, 2017, Lee *et al.*, 2020, Li *et al.*, 2022).

Hasanpour *et al.* (2017) employed VOF in presenting an analytical study of multiphase flow evaporation in an upward direction in a vertical tube using water. The study investigated characteristics of water flow boiling and achieving solid relationship between numerical and experimental HTC and found that increasing the velocity in the vapor phase led to noticeable fluctuations in HTC. Lee *et al.* (2020) went further with experiments that validated the numerical VOF model. The mechanism adopted was highly subcooled flow boiling of FC-72 (vertically) with data gotten from experiments at four different velocities. Various characteristics like patterns of flow regimes and heat transfer parameters were visualized to have a solid relationship with data from the corresponding experiments. The study focused on the effects and importance of thermohydraulic stability of flow boiling in a range of engineering applications found in heat exchangers, nuclear reactors, refrigeration systems, and high-performance electronic cooling systems. This can be noted as a superset of thermodynamics applications, like cooling systems, and micro-channel heat sinks (Ramesh *et al.*, 2021).

Focusing on microchannels with geometric modifications, this study follows a solid approach on how to mitigate most of these thermohydraulic instabilities. Altering the geometry, such as height, or cross-sectional area, contributes to influencing patterns of flow and stability (Karayiannis and Mahmoud, 2017).

This research aims to identify peak configurations that leads to thermohydraulic stability while consequently bolstering heat transfer performance, addresses practical challenges faced by engineers working with flow boiling in microchannel systems and the potential to unlock new possibilities for the design and implementation of efficient microscale thermodynamics systems. Furthermore, the VOF model has been compared to other models by researchers and with the advantages accomplished, the VOF model was chosen for this simulation. The findings of this study contribute to advancements in the fields like electronics cooling, microreactors, and microfluidics (Mudawar, 2011).

The objectives guiding the aim of this study include:

- i. Create a baseline rectangular geometry and run CFD simulations to analyse the pressure drop and HTC.
- ii. Modify the baseline geometry to constricted and expanding inlets and evaluate their impact on thermohydraulic performance through CFD simulations.
- iii. Visualize, compare and discuss results of the above geometries, identifying optimal specifications for enhancing thermohydraulic instability.

2.0 NUMERICAL METHODOLOGY

2.1 Problem Formulation

This study focuses on presenting an optimal microchannel to address thermohydraulic instabilities by setting a baseline rectangular microchannel and applying geometric modifications for comparison. These instabilities in form of pressure drop and heat transfer coefficient drives the need for this research study. The geometries simulated would be seen in Figures 1-3.

2.1.1 Case Geometries

This current work examines the following case geometry (baseline) in comparison with the modifications seeking to mitigate the instabilities employing water as the working fluid. The material the microchannel is made of is Aluminium (Al).

Table 1 shows the respective parameters for each case geometry.

Case 1 is a rectangular microchannel with the dimensions of the inlet same as that of the outlet (Figure 1). Case 2 differs from case 1 because it is restricted at the inlet but of the same exit size like case 1 (Figure 2). Further modification is done on case 1 to get case 3 which is a diverging microchannel at varying angle from the inlet to the outlet (Figure 3).

As seen, the modifications for case 2 are applied at the inlet with the fin thickness increased from 50 to 130 μm and as a result, the channel width is reduced from 200 to 40 μm . Using this modification, it is necessary to increase the mass flux in the channel to a higher value (5000 $\text{kg}/\text{m}^2\text{s}$) to enable adequate flow at the inlet.

Similarly, for the expanding inlet case geometry, the channel is modified back to its original fin thickness, but the channel is diverged at an angle 1° causing the height at the inlet to vary from that of the outlet (250 μm and 424 μm respectively). Same applies to the substrate thickness as would be seen in the figures below.

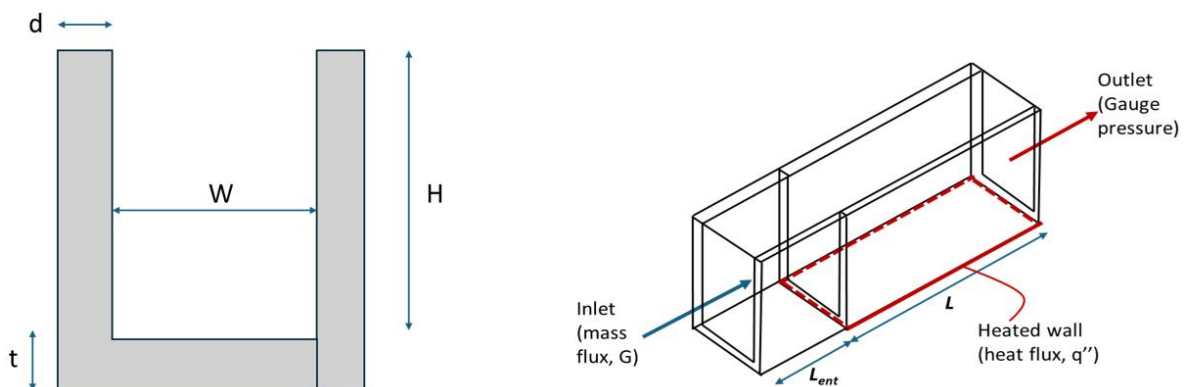


Fig 1. Geometry for the baseline rectangular microchannel (Case 1) showing the front and 3D view

Table 1. Dimensions of the case geometries and Boundary conditions

Parameter	Case 1	Case 2	Case 3	Boundary condition
Heated section length, L (mm)	10.5	10.5	10.5	
Adiabatic entrance length, L_{ent} (mm)	0.5	0.5	0.5	
The fin height, H (μm)	250	250	250	Inlet
			424	Outlet
The fin thickness, d (μm)	50	130	50	
The substrate thickness, t (μm)	50	50	224	Inlet
			50	Outlet
The channel width, W (μm)	200	40	200	
Total width, $W+2d$ (μm)	300	300	300	
Mass flux, G ($\text{kg}/\text{m}^2\text{s}$) at inlet	1000	5000	1000	
Gauge Pressure (Pa)	0	0	0	Outlet
Backflow temperature (K)	373.15	373.15	373.15	
Reynolds number, Re_L	790	790	790	
Prandtl number, Pr (Water)	1.74	1.74	1.74	
Heat flux, q'' (W/cm^2)	200	200	200	Bottom of the channel

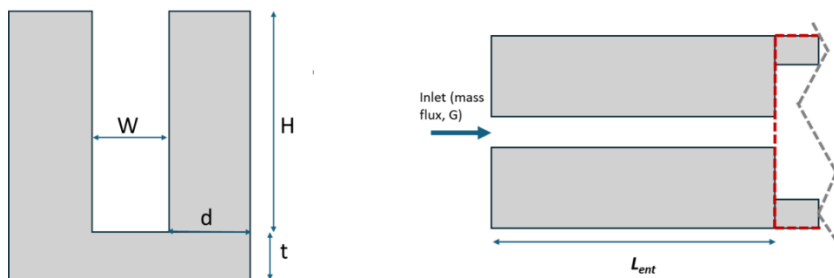


Fig 2. Geometry for the constricted inlet microchannel (case 2) showing the front and top views

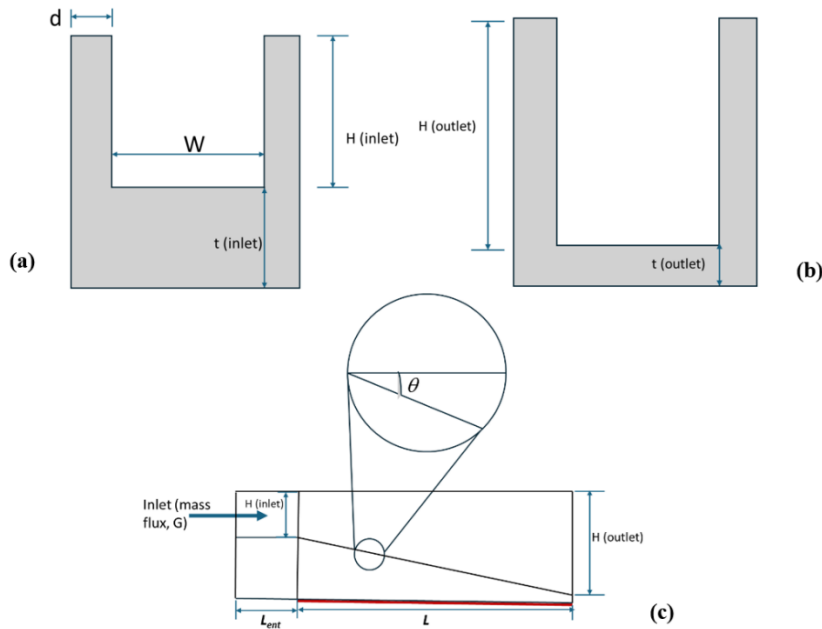


Figure 3. Geometry for the expanding and diverging microchannel $\theta = 1^\circ$ (Case 3) showing (a) inlet, (b) outlet, and (c) side profile

2.2 Numerical Procedure

Each configuration of the microchannels was subjected to CFD simulation to investigate influence of thermohydraulic properties on the varying dimensions (Table 1), analyze and virtualize heat transfer performance in terms of pressure drop and heat transfer coefficient as a

constant heat flux was applied to the bottom of the microchannel at varying mass flux at inlet. The simulations and mesh generation were carried out using the ANSYS Fluent, and Volume of Fluid (VOF) model. The flow is transient and laminar in a 3-D domain and discretized using the least squares cell-based method with a time step size of 2×10^{-7} s. Working fluid used is water (H_2O -liquid) with surface tension coefficient ($\sigma = 0.05894$), Courant number (Co) of 0.25, and saturation temperature at 373.15 K.

The convergence criteria for mass, momentum and, energy equations were set as 10^{-3} , 10^{-3} , and 10^{-6} respectively. For the Volume of Fluid (VOF) model, a Courant number (Co) of 0.25 default was maintained with a time step of 1.

2.3 Governing Equations

2.3.1 Mass conservation equation

For two fluids (liquid and vapor), the principle of conservation of mass is expressed in the equations below:

$$\frac{\partial}{\partial t}(\alpha_l \rho_l) + \nabla(\alpha_l \rho_l \vec{v}_l) = 0 \quad (1)$$

$$\frac{\partial}{\partial t}(\alpha_v \rho_v) + \nabla(\alpha_v \rho_v \vec{v}_v) = 0 \quad (2)$$

where,

α_l and α_v are volume fractions, ρ_l and ρ_v are densities, \vec{v}_l and \vec{v}_v are velocity vectors of respective mass transfer in each phase (evaporation and condensation).

Note: The equation below is the relationship between the liquid and vapor phase' volume fraction:

$$\alpha_l + \alpha_v = 1 \quad (3)$$

2.3.2 Momentum conservation equation

The momentum conservation is described as:

$$\frac{\partial}{\partial t}(\alpha_l \rho_l \vec{v}) + \nabla(\alpha_l \rho_l \vec{v} \vec{v}) = -\nabla P + \nabla[\mu_l \nabla \vec{v}_l + \nabla \vec{v}_l^T] + \rho_l \vec{g} + \vec{F} \quad (4)$$

$$\frac{\partial}{\partial t}(\alpha_v \rho_v \vec{v}) + \nabla(\alpha_v \rho_v \vec{v} \vec{v}) = -\nabla P + \nabla[\mu_v \nabla \vec{v}_v + \nabla \vec{v}_v^T] + \rho_v \vec{g} + \vec{F} \quad (5)$$

∇P is pressure change, μ_l and μ_v are dynamic viscosities of each phase, \vec{F} is body force, \vec{g} is gravity.

2.3.3 Equation for energy conservation

The energy conservation equation for the two phases is outlined as:

$$\frac{\partial}{\partial t}(\rho E) + \nabla[\vec{v}(\rho E + P)] = \nabla(k \nabla T) + S_e \quad (6)$$

S_e is source term (volumetric), k is thermal conductivity, ∇T is the temperature gradient and E is total energy per unit mass.

Further expressed as:

$$E = \frac{\alpha_l \rho_l E_l + \alpha_v \rho_v E_v}{\alpha_l \rho_l + \alpha_v \rho_v} \quad (7)$$

E_l and E_v are total energy per unit mass of respective mass transfer in each phase.

2.3.4 Surface tension model

To model for the surface tension forces, the continuum surface model was adopted. The surface tension forces are particularly important in the study of multiphase flows in small channels due to their dominance over gravitational and inertial forces, significantly influencing flow regimes and hydrodynamics (Vachaparambil and Einarsrud, 2019).

The equation governing this model comprises surface tension coefficient (σ) and two principal radii of curvature at a point on the curved surface (R_1 and R_2)

$$\Delta P = \sigma \left(\frac{1}{R_1} + \frac{1}{R_2} \right) \quad (8)$$

The **heat transfer coefficient** was determined using:

$$HTC = \frac{q''}{T_{sat} - T_{wall}} \quad (9)$$

where,

HTC is heat transfer coefficient, q'' is heat flux applied and, T_{sat} and T_{wall} are saturation and wall temperature respectively. Values for the wall temperature are obtained from simulations of the various geometries to help with this computation.

The **Nusselt number (Nu)** is further calculated from each simulation using:

$$Nu = \frac{HTC \times L}{k_f} \quad (10)$$

where, L = characteristic length of the microchannel, and k_f = fluid's thermal conductivity.

The **friction factor (fr)** was calculated using:

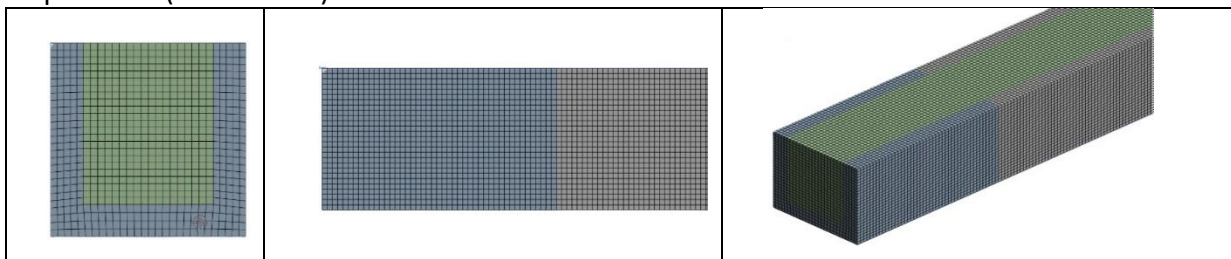
$$fr = \frac{\rho \times \Delta P}{2 \times G^2} \quad (11)$$

G = mass flux. The pressure drop is obtained from each simulation to help with this computation.

3.0 MESH INDEPENDENCE

A mesh/grid independence study was performed with the baseline geometry using the hexahedral meshing method. For a successful mesh study, improving accuracy and ensuring convergence is necessary. With every finer mesh iteration, different element sizes were obtained under same operating conditions (Fig. 4). The Tables 1-7 show the peak values attained for the pressure drop and the wall temperature which were the focus of comparison for all case geometries (case 1 – case 3). For clearer insights, the percentage change in the pressure drop and temperature were calculated and tabulated with a set criterion of <1% change chosen as an adequate basis for mesh independence.

The wall temperature is simulated with a boundary condition of constant saturation temperature (see Table 1)



(a)	(b)	(c)
<i>Figure 4. Mesh generated viewed in (a) cross-sectional (b) side (c) isometric</i>		

The significance of this mesh independence establishes a more precise and accurate converging result for the pressure drop, wall temperature and the calculation of the HTC, *Nu* and *fr*.

Case 1

Case 1, a rectangular microchannel, served as a baseline geometry for the initial simulations carried out. From Table 2 and Table 3, accurate results were obtained from the simulations using an element size of 756,000.

Table 2. Grid Independence analysis for the pressure drop

Elements	Pressure drop (KPa)	$ (\Delta P^k - \Delta P^{k+1})/(\Delta P^k) \times 100\%$
132000	16.35	7.84960
293200	15.16	13.51968
363132	17.53	0.62358
573125	17.64	0.56370
756000	17.74	-

Table 3. Grid Independence analysis for the temperature

Elements	Wall temperature (K)	$ (T_w^k - T_w^{k+1})/(T_w^k - 373) \times 100\%$
132000	332.59	8.52458
293200	328.82	5.12254
363132	326.44	2.45267
573125	325.27	0.25182
756000	325.15	-

Case 2

The case 2 geometry is a modification of case 1 which helps to observe the influence of a smaller inlet in mitigating instabilities in the microchannel. Element size of 998,280 was selected to get the most accurate results in simulations as seen in Table 4 and Table 5.

Table 4. Grid Independence analysis for the Pressure drop

Elements	Pressure drop (KPa)	$ (\Delta P^k - \Delta P^{k+1})/(\Delta P^k) \times 100\%$
200223	23.79	1.6667
282906	23.40	0.6369
336271	23.55	7.5746
435017	25.48	8.0144
747365	27.70	1.3533
955774	28.08	0.7072
998280	28.28	-

Table 5. Grid Independence analysis for the temperature

Elements	Wall temperature (K)	$ (T_w^k - T_w^{k+1})/(T_w^k - 373) \times 100\%$
200223	333.12	0.2037
282906	333.80	0.0329
336271	333.91	0.2092
435017	334.61	0.0568
747365	334.42	0.0329
955774	334.53	0.0628
998280	334.32	-

Case 3

The case 3 provides more insights into microchannels with diverging inlet at a given angle and how they further affect the performance of the system in terms of heat transfer coefficient and pressure drop. Element size of 847,813 was selected to get the most accurate results in simulations as seen in Table 6 and Table 7.

Table 6. Grid Independence analysis for the pressure drop

Elements	Pressure drop (KPa)	$ (\Delta P^k - \Delta P^{k+1})/(\Delta P^k) \times 100\%$
156770	5.02	14.7708
298036	5.89	5.3055
455688	6.22	2.5078
688569	6.38	0.4680
847813	6.41	-

Table 7. Grid Independence analysis for the temperature

Elements	Wall temperature (K)	$ (T_w^k - T_w^{k+1})/(T_w^k - 373) \times 100\%$
156770	330.53	1.9926
298036	337.25	0.6949
455688	339.61	1.1325
688569	343.50	0.0785
847813	343.77	-

4.0 RESULTS AND DISCUSSION

Table 8 shows the values obtained for the CFD simulation (HTC and pressure drop) for all cases in comparison with Broughton and Joshi (2021). The values for the Mean Absolute Deviation (MAD) are computed using the correlation in the work of Osowade *et al.*, (2024) as:

$$M.A.D = \frac{1}{N} \sum_1^N ABS \left[\frac{i_{predicted} - i_{numerical}}{i_{numerical}} \times 100\% \right] \quad (12)$$

Table 8. Comparison of the HTC and pressure drop with Broughton and Joshi (2021)

Case	Broughton and Joshi (2021)	Current study	AD (%)	Broughton and Joshi (2021)	Current study	AD (%)
	h_{tp} (kW/m ² K)	h_{tp} (kW/m ² K)		P (kPa)	P (kPa)	
1	49.50	41.67	15.82	19.32	17.74	8.18
2	51.10	51.51	0.80	25.30	28.28	11.78
3	61.50	68.07	10.68	8.21	6.41	21.92
	M.A.D (%)		9.1			13.96

The results obtained for the Mean Absolute Deviation as seen in Table 8 explains the close correlation between the simulation of this study and that of Broughton and Joshi (2021) with the closest being case 2 of 0.8 % absolute deviation for the HTC and case 1 of 8.18 % absolute deviation for the pressure drop. This further validates the steps followed, as well as the simulation setup employed in the current study.

Figure 5 shows the agreement of the HTC obtained from the simulation in this current study, plotted alongside the values of Broughton and Joshi (2021). As shown in Figure 5, there is a significant increase in HTC of the microchannel with the expanding inlet (case 2) giving a better heat transfer characteristic. This is because the expanding inlet promotes a better distribution and mixing of the fluid in comparison to the other geometries, thus reducing the thermal

boundary layer more effectively. Channel's divergence increases the surface area in which the fluid has contact.

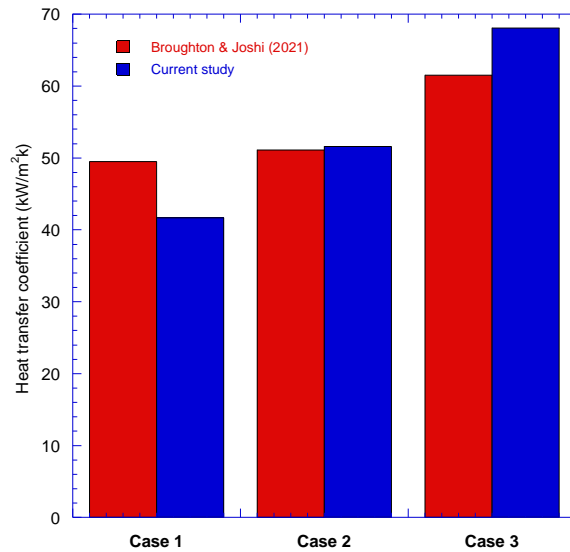


Figure 5. Graph showing the correlation of surface HTC.

Figure 6 shows the correlation between the pressure drop values for all three case geometries obtained from Broughton and Joshi (2021) and the current study. The result from the simulation in the current study is plotted alongside the values of Broughton and Joshi (2021). Similar to the HTC, the result in Figure 6 is supported by the values of the Mean Absolute Deviation calculated. Similarly, there is a significant increase in the pressure drop (case 2) and then a much larger decrease in pressure drop (case 3). This is attributed to the fact that in the baseline microchannel (case 1), the pressure drop is primarily due to the frictional losses along the channel walls. There are no abrupt changes in cross-sectional area to cause additional turbulence or energy losses. Thus, resulting in a moderate pressure drop value which reflects the balance between driving pressure and frictional forces.

In the constricted inlet (case 2), the area of the inlet is far smaller than that of the outlet. This consequently leads to a high velocity of the fluid entry, which leads to increase in kinetic energy in substitution for the pressure energy (described by the Bernoulli's principle). Due to this high velocity at the entry point, the flow accelerates, causing a significant drop in pressure at the narrow section. The overall result is a higher pressure drop (Figure 6) due to the combined effects of frictional losses and turbulence generated by the sudden expansion of the microchannel.

In contrast to the constricted inlet, the expanding inlet has a larger area at the inlet. This geometry design enables the fluid to decelerate smoothly as it moves through the channel, thus reducing the velocity and subsequently the turbulence. This minimizes the sudden changes in flow velocity, resulting in a significantly lower pressure drop.

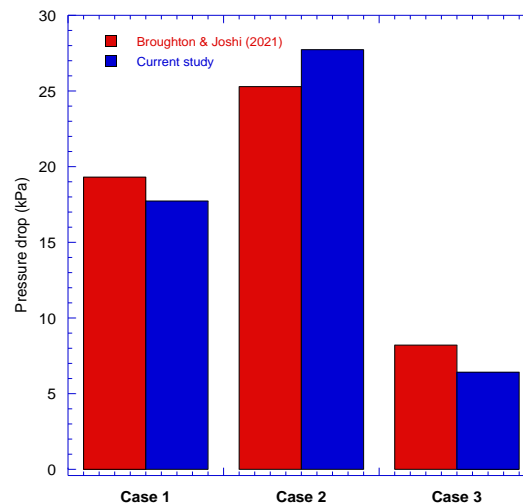


Figure 6. Graph showing the correlation of static Pressure drop.

In the section, the simulations are focused on varying mass flux and studying its effect on the thermohydraulic characteristics (Nusselt number and frictional factor).

Also, for the expanding inlet and diverging microchannel, the angle of divergence is varied to give a larger view and better understanding of the scope of this research.

4.1 Influence of varying mass flux' effect on the thermohydraulic characteristics

The mass flux effect on characteristics like HTC and PD for various case geometries was studied. These effects were determined by calculating for the frictional factor and Nusselt number. The frictional factor exhibits a downward trend with increasing mass flux for all case geometries as shown in Figure 7.

In the baseline rectangular micro-channel (case 1), the frictional factor decreases with a steady increase in mass flux. This is consistent with findings in Osowade *et al.*, (2024) where higher mass flux boosts convective heat transfer and depletes the significance of viscous forces, thus leading to lower frictional losses.

In the constricted inlet microchannel (case 2), a similar trend is observed with a range of mass flux (3000 – 7000 kg/m²s). Normah *et al.*, (2013) reported that constrictions in microchannels initially increase flow velocity and turbulence, enhancing heat transfer but also increasing frictional losses. However, the overall effect of increased turbulence reduces the relative viscous effects as mass flux increases. Thus, significantly decreasing the friction factor in alignment with the current study as seen in the Figure 7.

In the expanding inlet and diverging microchannel (case 3), the friction factor again shows a similar behaviour as mass flux increases. The friction factor decreases from 1.204 to 0.54 as G increases from 3000 to 7000 kg/m²s. This result is supported by the work of Lee *et al.*, (2007), who found that diverging microchannel designs promote smoother flow transitions and reduce turbulence and pressure drop more effectively at higher mass flux rates compared to baseline geometries. The expanding inlet design helps stabilize the flow, reducing frictional losses more efficiently at higher mass fluxes.

There is a 33.47 % difference in the pressure drop for case 1, 59.38 % difference in the pressure drop for case 2, and 52.66 % difference in the pressure drop for case 3. This implies that there is a significantly better performance in case 2 for the pressure drop when compared to case 1 and case 3.

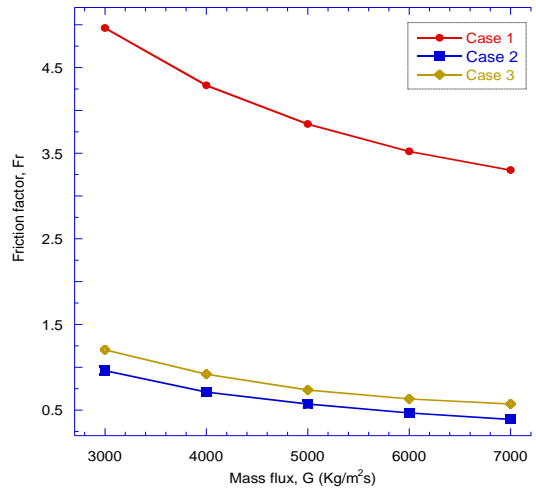


Figure 7. Friction factor against mass flux, *G* for all cases

Figure 8 shows the relationship between Nusselt number and varying mass flux, *G*. As seen in the Figure 8, Nusselt number reduces as mass flux is increased in all case geometries.

In the cases 1 and 3, while increasing the mass flux generally enhances turbulence and convective heat transfer, other factors such as flow instabilities or the formation of a vapor layer can diminish the overall heat transfer efficiency at higher mass flux, thus leading to a smaller value for Nusselt number.

In the constricted inlet microchannel (case 2), the Nusselt number significantly decreases as mass flux increased. High Nusselt number can be attributed to the constriction causing a rapid increase in flow velocity and turbulence, enhancing heat transfer (Broughton and Joshi, 2021). However, with a steady increase in mass flux, the benefits of this turbulence can be outweighed by factors like increased pressure drop and flow maldistribution. These effects lead to reduction in Nusselt number.

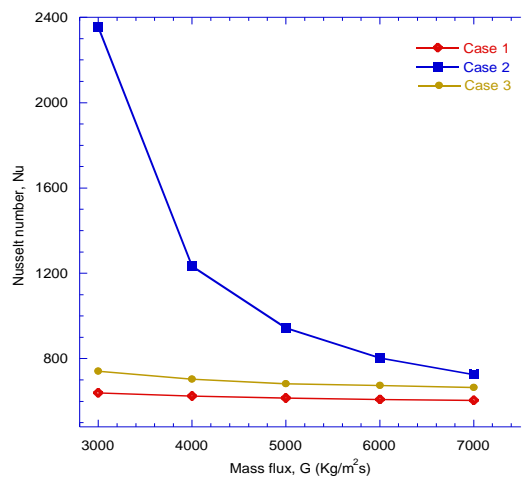


Figure 8. Nusselt number, *Nu* against mass flux, *G*

4.2 Influence of varying angle of divergence on the thermohydraulic characteristics of the diverging microchannel

Figure 9 shows a broader relationship between the Nusselt number and the mass flux range 3000 – 7000 kg/m²s at varying angles of divergence. The relationship follows the same trend in all angles of divergence, i.e., a decrease in Nusselt number as mass flux increases.

At each mass flux, the Nusselt number decreases with approximately 0.25 %, 0.9 %, 1 %, 3 % as the angle of divergence increases respectively.

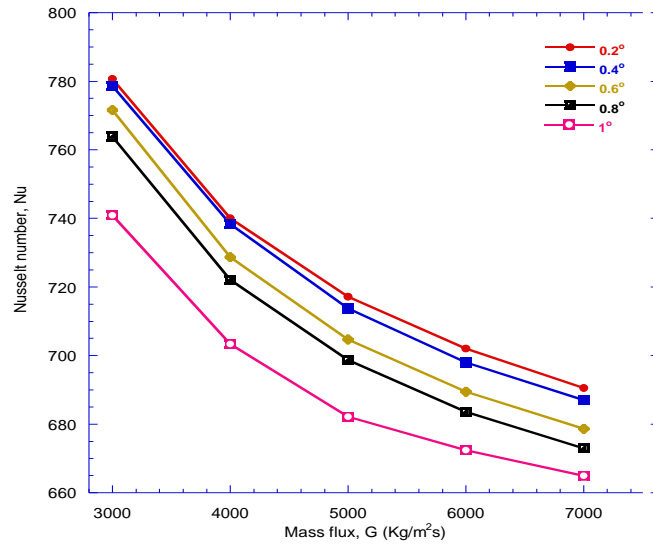


Figure 9. Nusselt number, Nu against mass flux, G at varying angle of divergence

Figure 10 presents the relationship between friction factor and the varying mass flux of 3000 – 7000 kg/m²s at different angle of divergence. It is clear from Figure 10 that frictional factor decreases as mass flux increases at increasing angle of divergence. This implies that the more the working fluid passed into the microchannel, the lesser the pressure drop and consequently, the frictional factor. At each mass flux, the friction factor decreases with approximately 9 %, 11 %, 10 %, 7 % as the angle of divergence increases respectively.

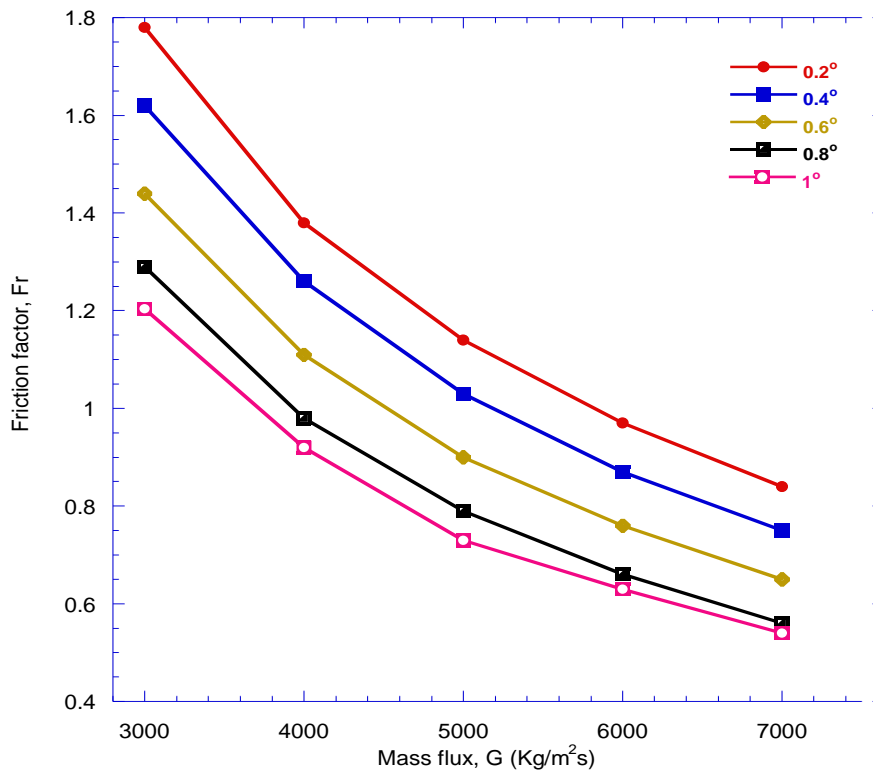


Figure 10. Friction factor, fr against mass flux, G at varying angle of divergence

Figure 11 shows that at varying mass flux, the friction factor reduces as the angle of divergence is increased. The angle of divergence further explains the area of contact of the working fluid

and the microchannel. Similar to the analysis on Fig 9 & 10, the higher the mass flux, the better the pressure drop within the microchannel.

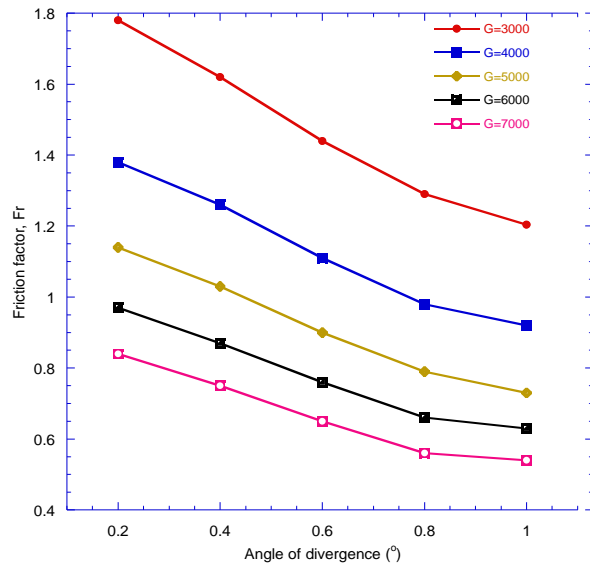


Figure 11. Frictional factor, f_r against angle of divergence ($^\circ$) at varying mass flux

Figure 12 shows the relationship between convective heat transfer, that is the Nusselt number and the varying angle of divergence at different mass flux. This further strengthens the relationship seen in Figure 9 that increasing mass flux decreases the heat amount transferred in the fluid. As is the aim to reduce the thermohydraulic instabilities in the microchannel, more mass flux would yield a better conductive heat transfer between the fluid and the microchannel.

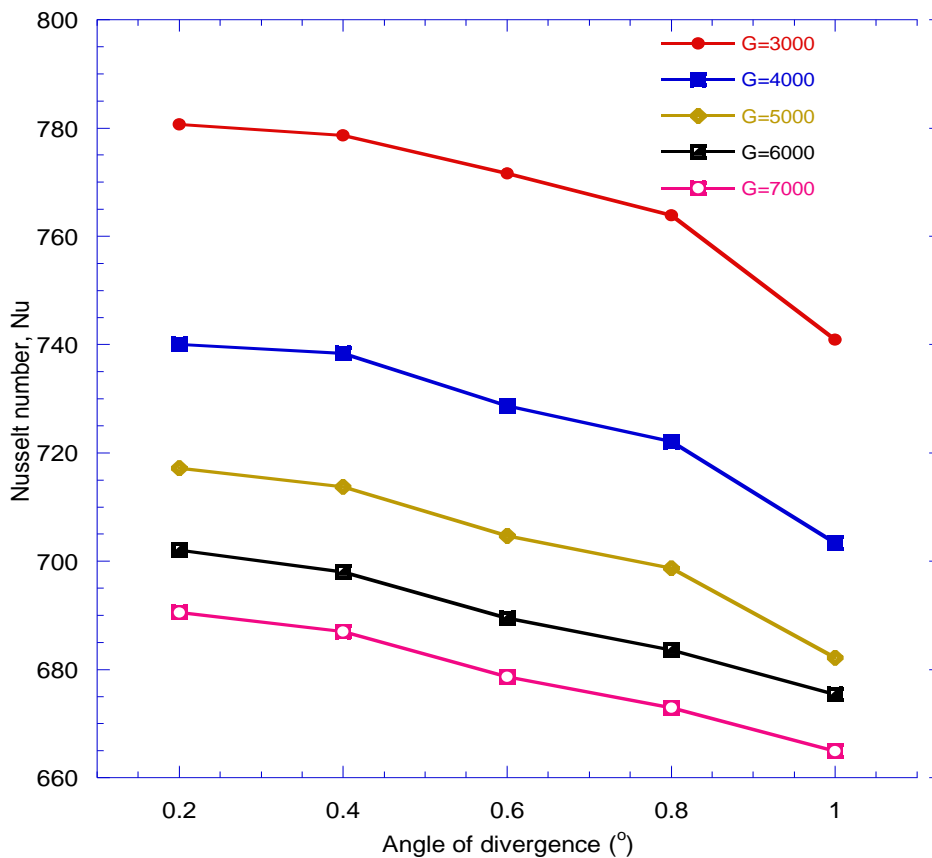


Figure 12. Nusselt number, Nu against angle of divergence ($^\circ$) at varying mass flux

5.0 CONCLUSION

This study was conducted using geometric modifications, which successfully investigated thermohydraulic instabilities in microchannels, and ANSYS CFD simulation was run employing the Volume of Fluid (VOF) model. Encompassed within these were a mass flux range of 3000 – 7000 kg/m²s and an angle of divergence of 0.2^o – 1^o, while the heat flux was kept constant at a value of 200 W/cm². With these, calculations and visualizations were used to determine what effects the Nusselt number and frictional factor had on the different microchannels. In the case of an expanding inlet and diverging microchannel, it caused a dramatic surge in the heat transfer coefficient value to about 68.07 kW/m²K against the background value of 41.67 kW/m²K obtained for Case 1, which is a purely rectangular geometry. Secondly, Case 3 returned a drop in pressure to a more acceptable value of 6.41 kPa from 17.74 kPa, as was obtained in Case 1. These results suggest that expanding geometries at the inlet will enhance heat transfer with reduced pressure losses. For the constricted inlet design, though HTC increased to about 51.51 kW/m²K in Case 2, the pressure drop surged to 28.28 kPa, which is an indication that this set will increase flow resistance. That essentially means that while a constricted inlet design may turn out useful for instances where heat transfer is paramount over pressure drop, it would not be very feasible in applications sensitive to pressure losses. In other words, the research realizes that optimization in microchannel performance relies on geometric modifications; in this case, the expanding inlet design will be most effective with respect to balancing heat transfer and pressure drop. The results clearly point one to future direction of studies in microchannel design and optimization, more so in high-performance cooling systems.

ACKNOWLEDGEMENT

The success of this research would not have been possible without the facilities provided at the Royal Society Research Laboratory in the University of Lagos, Akoka. The efforts made and procedures put in place by the management of the research lab is wholly appreciated and acknowledged.

REFERENCES

- Adio, S. A., Olalere, A. E., Olagoke, R. O., Alo, T. A., Veeredhi, V. R., Ewim, D. R. E., Olakoyejo, O. T. (2021). Thermal and entropy analysis of a manifold microchannel heat sink operating on CuO-water nanofluid. *Journal of the Brazilian Society of Mechanical Sciences and Engineering*. <https://doi.org/10.1007/s40430-020-02772-x>
- Balasubramanian, K., Lee, P. S., Jin, L. W., Chou, S. K., Teo, C. J., and Gao, S., (2011). Experimental investigations of flow boiling heat transfer and pressure drop in straight and expanding microchannels—A comparative study, *Int. J. Therm. Sci.* 50(12), Pages1 2413–2421.
- Balasubramanian, K.R., Peter, R., & Krishnan, R.A. (2022). Recent hypotheses on the parameters of microchannel flow boiling: a comprehensive overview. *Microfluidics and Nanofluidic*, Page 26.
- Broughton, J., and Joshi, Y. K. (2021). Flow boiling in geometrically modified microchannels. *Physics of Fluids* 33, 103308. <https://doi.org/10.1063/5.0062585>
- Cukrov, A., Tuković, Ž., Ničeno, B., Boras, I., Galović, A. (2017). On Mixture Model Application in Numerical Modelling of Boiling Phenomena, in *24th International Symposium on Heating, Refrigerating and Air Conditioning*. Pages 1–7.
- Hasanpour, B., Irandoost, M.S., Hassani, M. (2017). Numerical investigation of saturated upward flow boiling of water in a vertical tube using VOF model: effect of different boundary conditions. *Heat Mass Transfer*, Volume 54, Pages 1925 – 1936. <https://doi.org/10.1007/s00231-018-2289-3>
- Hasselgreaves, J. E., Law, R., Reay, D. A. (2016). *Compact heat exchangers: selection, design, and operation: Second Edition*
- Jia, Y. T., Xia, G. D., Zong, L. X., Ma, D. D., Tang, Y. X. (2018). A comparative study of experimental flow boiling heat transfer and pressure drop characteristics in porous-wall microchannel heat sink. *International Journal of Heat and Mass Transfer*, Volume 127, Pages 818-833.

- Kamel, M. S., Lezsovits, F., Hussein, A. K. (2019). Experimental studies of flow boiling heat transfer by using nanofluids. *Journal of Thermal Analysis and Calorimetry*, Page 138: 4019-4043. <https://doi.org/10.1007/s10973-019-08333-2>
- Karayiannis, T., & Mahmoud, M. (2017). Flow boiling in microchannels: Fundamentals and applications. *Applied Thermal Engineering*, Page 115, 1372-1397. <https://doi.org/10.1016/j.applthermaleng.2016.08.063>
- Karayiannis, T., & Mahmoud, M. (2018). Flow boiling in micro-passages: Developments in fundamental aspects and applications.
- Kumar, A., Singh, S., & Tiwari, A. K. (2021). Experimental investigation of flow boiling heat transfer in microchannels using water-CuO nanofluids. *Journal of Thermal Analysis and Calorimetry*, 155(1), Page 547-562. <https://doi.org/10.1007/s10973-020-09855-1>
- Lee, J., O'Neill, L., Mudawar, I. (2020). Computational prediction of key heat transfer mechanisms and hydrodynamic characteristics of critical heat flux (CHF) in subcooled vertical upflow boiling. *International Journal of Heat and Mass Transfer*, Volume 161, 120262, ISSN 0017-9310. <https://doi.org/10.1016/j.ijheatmasstransfer.2020.120262>.
- Lee, P & Pan, C. (2007). Boiling heat transfer and two-phase flow of water in a single shallow microchannel with a uniform or diverging cross section. *Journal of Micromechanics and Microengineering*. 18. 025005. 10.1088/0960-1317/18/2/025005.
- Li, H., Wang, Z., Zhang, H., & Chen, X. (2022). Experimental investigation of flow boiling heat transfer enhancement using hybrid nanofluids. *Experimental Thermal and Fluid Science*, Page 136, 110693. <https://doi.org/10.1016/j.expthermflusci.2022.110693>
- Li, H., Wang, L., Zhang, H., & Chen, X. (2023). Experimental investigation of flow boiling heat transfer enhancement using carbon nanotube nanofluids. *International Journal of Heat and Mass Transfer*, Page 187, 121086. <https://doi.org/10.1016/j.ijheatmasstransfer.2023.121086>
- Liu, H., Chen, L., Lin, Z., & Fang, X. (2022). Investigation of flow boiling heat transfer and pressure drop in a small-scale serpentine microchannel. *International Journal of Multiphase Flow*, Page 143, 103741. <https://doi.org/10.1016/j.ijmultiphaseflow.2022.103741>
- Liu, Y., Wang, Z., Zhang, Q., & Lin, S. (2023). Investigation of flow boiling heat transfer characteristics in multi-port microchannels. *International Journal of Heat and Mass Transfer*, Page 188, 121124. <https://doi.org/10.1016/j.ijheatmasstransfer.2023.121124>
- Ma, X., Ji, X., Wang, J., Fang, J., Zhang, Y., Wei, J. (2022). Flow boiling heat transfer characteristics on micro-pin finned surfaces in a horizontal narrow microchannel. *International Journal of Heat and Mass Transfer*, Volume Page 194, 123071, <https://doi.org/10.1016/j.ijheatmasstransfer.2022.123071>
- Mohammed, H. I., Griddings, D., Walker, G. S. (2019). CFD multiphase modelling of the acetone condensation and evaporation process in a horizontal circular tube, *International Journal of Heat Mass Transfer*, 134, Page 1159-1170. <https://doi.org/10.1016/j.ijheatmasstransfer.2019.02.062>
- Mudawar, I. (2011). Two-phase micro-channel heat sinks: theory, applications, and limitations, *ASME. J. Electron. Packag*; 133(4): 041002 <https://doi.org/10.1115/1.4005300>
- Mudawar, I. (2013). Recent advances in high-flux, two-phase thermal management, *ASME. J. Therm. Sci. Eng. Appl.* 5(2): 021012. <https://doi.org/10.1115/1.4023599>
- Mukherjee, A. & Kandlikar, S. G., (2009). Numerical simulation of growth of a vapor bubble during flow boiling of water in a microchannel. *Microfluidics and Nanofluidics*, 1(2):137-145. <http://dx.doi.org/10.1007/s10404-004-0021-8>
- Normah & Ahmad, Robiah, Adham, Ahmed & Mohd-Ghazali, (2013). Thermal and hydrodynamic analysis of microchannel heat sinks: A review. *Renewable and Sustainable Energy Reviews*.
- Oswade, E. A., Adelaja, A. O., Olakoyejo, O. T., Obayopo, S. O., Tryggvason, G., Meyer, J. P. & Markides, C. N. (2024). Numerical investigation of flow boiling characteristics of R134A in a smooth horizontal tube, *International Journal of Heat and Mass Transfer*.
- Özdemir, M. R. & Sozbir, Ö.R. (2018). A review of single-phase and two-phase pressure drop characteristics and flow boiling instabilities in microchannels.
- Ramesh, K.N., Sharma, T.K. & Rao, G.A.P. (2021). Latest Advancements in Heat Transfer Enhancement in the Micro-channel Heat Sinks: A Review. *Arch Computat Methods Eng* 28, 3135–3165. <https://doi.org/10.1007/s11831-020-09495>
- Soliman, A. M. A., Abdel Rahman, A. K., Ookawara, S. (2018). Enhancement of vapor compression cycle performance using nanofluids: experimental results. *J Therm Anal Calorim*.
- Sun, D., Xu, J., Chen, Q. (2014). Modelling of the evaporation and condensation phase-change problems with FLUENT, *Numerical Heat Transfer, Part B: Fundamentals*. 66, Page 326-342. <https://doi.org/10.1080/10407790.2014.915681>

- Vachaparambil, K. & Einarsrud, K. (2019). Comparison of surface tension models for the volume of fluid (VOF) method. Department of Materials Science and Engineering, Volume 7 (8), 542. <https://doi.org/10.3390/pr7080542>
- Wang, J., Wu, J., & Yang, L. (2021). Study on the flow boiling heat transfer performance of R134a in a microchannel heat sink with different channel orientations. *Heat Transfer Research*, 52(7), Page 601-617. <https://doi.org/10.1615/HeatTransRes.2021040586>
- Wang, Y., Li, S., & Zhang, W. (2023). Study on the characteristics of flow boiling heat transfer of R410A in a horizontal smooth tube. *International Journal of Refrigeration*, Page 125, 109-120. <https://doi.org/10.1016/j.ijrefrig.2022.12.005>
- Wang, Z., Liu, X., Zhang, Q., & Zhao, J. (2021). Comparative study of flow boiling heat transfer enhancement using structured and plain microchannels. *Heat Transfer Engineering*, 42(13), Page 1121-1132. <https://doi.org/10.1080/01457632.2020.1833332>
- Wlazlak, A., Zajaczkowski, B., Woluntarski, M., Buschmann, M. H. (2018). Influence of graphene oxide nanofluids and surfactant on thermal behaviour of the thermosyphoon. *J. Therm Anal Calorim.* <https://doi.org/10.1007/s10973-018-7632-x>
- Yogesh K. Prajapati, Manabendra Pathak, Mohd. Kaleem Khan (2017). Numerical investigation of subcooled flow boiling in segmented finned microchannels. *International Communications in Heat and Mass Transfer*, Volume 86, 2017, Pages 215-221, ISSN0735-1933. <https://doi.org/10.1016/j.icheatmasstransfer.2017.06.009>.
- Zhang, J., Zeng, S., Tang, Y., Sun, Y., Yuan, W. (2017). Flow boiling characteristics of micro-grooved channels with re-entrant cavity array at different operational conditions. *International Journal of Heat and Mass Transfer*, Page 114, 1001-1012. <https://doi.org/10.1016/j.ijheatmasstransfer.2017.06.128>.

APPENDIX

Fig A1 and A2 show the contour of the heat transfer coefficient and pressure drop for the research study investigated.

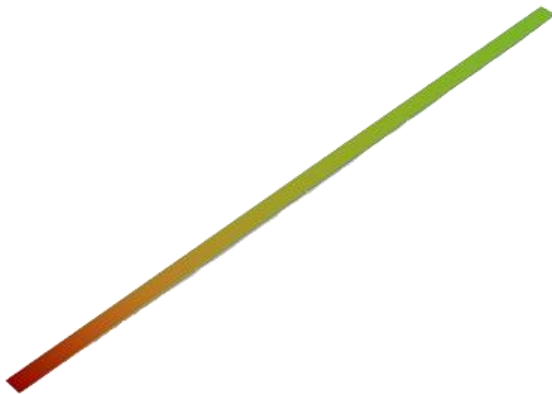


Fig A1. Contour for Heat transfer coefficient

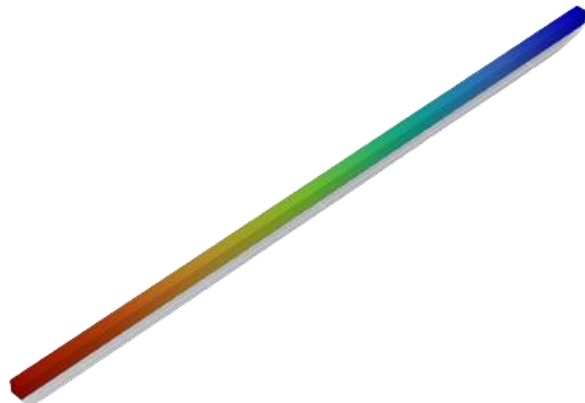


Fig A2. Contour for pressure drop